Effect of temperature and pH on phase transformations in citric acid-mediated hydrothermal growth of tungsten oxide

Kasper Wenderich,*[a, b] Johannes Noack,[c, d] Anne Kärgel,[c] Annette Trunschke[c] and Guido Mul[a]

Abstract: The temperature dependent composition of suspension during citric acid-mediated crystallization of tungsten trioxide (WO_3) from sodium tungstate was studied by *in situ* Raman spectroscopy. Additionally, microwave-assisted hydrothermal synthesis experiments combined with *ex situ* analysis by X-Ray diffraction and Scanning Electron Microscopy were performed to analyze the effect of pH on the eventually, isothermally, obtained crystal phase and morphology. The Raman results suggest that $WO_3 \cdot 2H_2O$ precipitates from the tungstate solution upon acidification to pH 0.5 at room temperature. This is first transformed to $WO_3 \cdot H_2O$ initiating at T = 70 °C. At temperatures above 170 °C, the crystallization of phase-pure monoclinic WO_3 with well-defined plate-like morphology was observed at pH 0.5. Using the microwave-assisted hydrothermal synthesis procedure shows that increasing the pH to values of 1.5 or 2 results in significant or dominant formation of hexagonal WO_3, respectively. Comparing the activity of selected samples in photocatalytic oxidation of propane using visible light, demonstrates the presence of hydrate phases or hexagonal WO_3 is detrimental to performance.

Introduction

One of the most studied semiconductor materials in various applications (optics, sensors, catalysts), is tungsten trioxide (WO_3). WO_3 is chemically stable, non-toxic and has a relatively small bandgap (ranging from 2.4 to 2.8 eV).[1] Due to the latter property, WO_3 is able to absorb visible light in the blue range of the visible spectrum, and able to induce photocatalytic transformations, such as in waste water treatment, and in water decomposition when part of a Z-scheme configuration.[2] Methods to synthesize WO_3 include sol-gel methods,[3] solvothermal synthesis,[4] electrochemical etching,[5] spray pyrolysis,[6] chemical vapor deposition,[7] and template directed synthesis.[8] The hydrothermal synthesis route gives access to WO_3 particles with a well-defined morphology, such as nanorods,[9] nanowires,[10] nanoplates/nanosheets,[11] nanocubes,[11c] octahedra,[12] nano-urchins[10b, 13] and flower-like morphologies.[14] Often capping agents are used to control the morphology and crystal phase of the samples. These capping agents adsorb on specific surface facets of a crystal during hydrothermal growth, and thus influence the final morphology.[15] Although citric acid-mediated growth of plate-like WO_3 in microwave-assisted hydrothermal synthesis has been reported previously by Sungpanich *et al.*,[16] a detailed analysis of the effect of process conditions during synthesis (pH and temperature) on the growth mechanism and obtained crystal phase and morphology, has not yet been reported.

In this work, the phase transitions of tungstates initiated by acidification and increasing temperature up to 170 °C, were investigated by *in situ* Raman spectroscopy.[17] Additionally, microwave-assisted hydrothermal synthesis experiments combined with *ex situ* analysis by X-Ray diffraction and Scanning Electron Microscopy were performed to in particular analyze the effect of pH on morphology and phase composition of the final product after extended isothermal crystallization time, reduced from 17 hours in the Raman-autoclave to 2 hours in the microwave methodology. Finally, a selected number of WO_3 samples obtained by microwave-assisted hydrothermal synthesis were tested for their photocatalytic activity through the oxidation of propane,[18] to determine the WO_3 phase providing optimized performance.

Results and Discussion

In situ Raman spectroscopy of crystal phases during hydrothermal synthesis of WO_3

Figure 1 shows the Raman spectra in the typical range of ν(W=O), ν(O-W-O) and δ(O-W-O) vibrations measured during the heating stage of the hydrothermal reaction of sodium tungstate at a pH of 0.5 in the presence of citric acid, and up to a temperature of 170 °C. At room temperature, the acidification of the tungstate solution leads to the precipitation of tungstic acid. This formation can be observed by the Raman bands in the spectra.[19] In its monohydrate form ($WO_3 \cdot H_2O$), tungstic acid is composed of layers of octahedrally coordinated $WO_5(H_2O)$ units connected by 4 vertices in the plane. The dihydrate form ($WO_3 \cdot 2H_2O$) is structurally quite similar with additional water molecules

[a] Dr. K. Wenderich, Prof. Dr. G. Mul
Photocatalytic Synthesis Group, Faculty of Science and Technology
MESA+ Institute for Nanotechnology, University of Twente
PO Box 217, 7500 AE Enschede, The Netherlands
[b] Dr. K. Wenderich
Centre for Innovation Competence SiLi-nano®
Martin-Luther-University Halle-Wittenberg
Karl-Freiherr-von-Fritsch-Str. 3, 06120 Halle (Saale), Germany
E-mail: kasper.wenderich@chemie.uni-halle.de
URL: http://www.sili-nano.de/de/detail/kasper-wenderich.html
[c] Dr. J. Noack, A. Kärgel, Dr. A. Trunschke
Department of Inorganic Chemistry
Fritz-Haber-Institute der Max-Planck-Gesellschaft e.V.
Faradayweg 4-6, Berlin, Germany
[d] Dr. J. Noack
BasCat – UniCat BASF JointLab
Technische Universität Berlin
Sekr. EW K-01 Hardenbergstraße 36, 10623 Berlin, Germany

Supporting information for this article is given via a link at the end of the document.

intercalated between the layers. Both phases can be identified in the Raman spectra by their characteristic v(W=O) bands at 945 and 958 cm^{-1}, respectively. Additionally, bands from 632 to 650 cm^{-1} and at 884 cm^{-1} are found, which correspond to v(O-W-O) vibrations. While at low temperatures up to approximately 70 °C the dihydrate is the major phase, during heating of the solution, its bands gradually decrease in intensity for the benefit of the monohydrate. Starting from 150 °C, $WO_3 \cdot H_2O$ is consumed and bands at 806, 714, 323 and 269 cm^{-1} appear, indicating the formation of monoclinic WO_3. From those measurements, $WO_3 \cdot 0.33H_2O$ phase (which would exhibit intense bands at 945, 805, 680 cm^{-1}) as a possible intermediate in the transformation to monoclinic WO_3 is not clearly identified.[19c] Also, Raman bands from the citric acid acting as structure directing agent added in the synthesis are not observed (Figure S7). The XRD pattern of the precipitate after washing and drying (Figure S2) exclusively shows peaks corresponding to monoclinic WO_3.

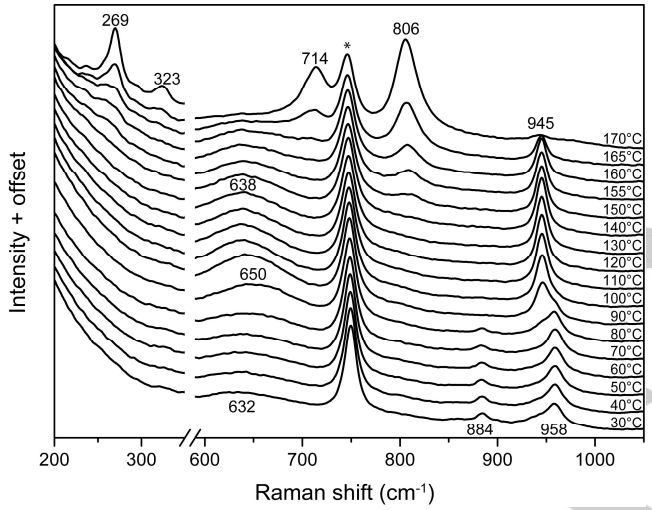

Figure 1. Raman spectra measured *in situ* during hydrothermal synthesis during the heating of an aqueous sodium tungstate solution (0.05 M) at pH = 0.5 in the presence of citric acid. The band at 746 cm^{-1} marked with * is assigned to the sapphire window of the Raman probe. The reaction temperature profile is given in Figure S1.

To further investigate the formation of monoclinic WO_3, experiments were conducted at 150 °C, which is the initial transformation temperature from the monohydrate to monoclinic WO_3. Also the pH was increased to a value of 1. A similar behavior is observed in this experiment compared to the previous one as seen from the *in situ* Raman spectra (Figure S3). Reaching 150 °C, the band at 806 cm^{-1} is increasing in intensity as a function of time, while the characteristic bands of the monohydrate phase at 945 and 639 cm^{-1} vanish. From 1 to 15 hours of reaction time, the absolute and relative intensities of the bands barely change, indicating complete phase transformation already occurred one hour after the isothermal point was reached. Again, the XRD pattern of the precipitate after washing and drying shows exclusively peaks corresponding to monoclinic WO_3 (Figure S4). Comparison of the Raman spectra in Figure 1, and Figure S3 reveals that in Figure 1 no sign of $WO_3 \cdot H_2O$ is observed at pH = 0.5 at low temperatures, while its existence is observed in Figure S3 in addition to the dihydrate, by the band at 945 cm^{-1}. This is likely due to the higher pH employed during the experiment shown in Figure S3. The SEM images of the two as-discussed experiments with 170 and 150 °C reaction temperatures (Figures S2 and S4) show plate-like particles exhibiting sharp edges, reflecting the monoclinic crystal structure of WO_3. This overall anisotropy in the particle dimensions is also observed in the XRD patterns by an under-estimation of the reflections involving the crystallographic a-axis and has thus been considered in the Rietveld fit-model.

Besides analysis of the final products, the transients observed in the *in situ* Raman experiments were complemented by XRD and SEM investigations of samples drawn from the hydrothermal vessel at different points during the hydrothermal reaction at 150 °C. The XRD patterns in Figure 2a show the formation of the monohydrate phase precipitating from the acidified solution of Na_2WO_4 at temperatures above 100 °C and its decomposition to monoclinic WO_3 starting at 150 °C. This phase transformation is best seen by decreasing intensity of the reflections at 2θ = 16.5, 25.6 and 52.7° and appearance of a trifold of reflections at 2θ = 23.1, 23.6 and 24.4°. As seen *e.g.* by the reflections at 2θ = 14.1° and 18.0° appearing after 1 hour of hydrothermal synthesis, little amounts of $WO_3 \cdot 0.33H_2O$ are formed in addition, which slowly decompose during the reaction at 150 °C. In the Raman spectra, these traces are not observed due to a strong overlap of the various bands. The SEM images (Figure 2b) of the samples drawn during heating at 130 °C and after 1, 7 and 17 h of isothermal reaction at 150 °C, reflect the transformation of the irregularly shaped hydrate phase into the nicely defined rectangular shape of the final monoclinic WO_3. Defects in the crystal morphology are reduced and the mean particle size gets more uniform as a result of Ostwald ripening with increasing reaction time at 150 °C.

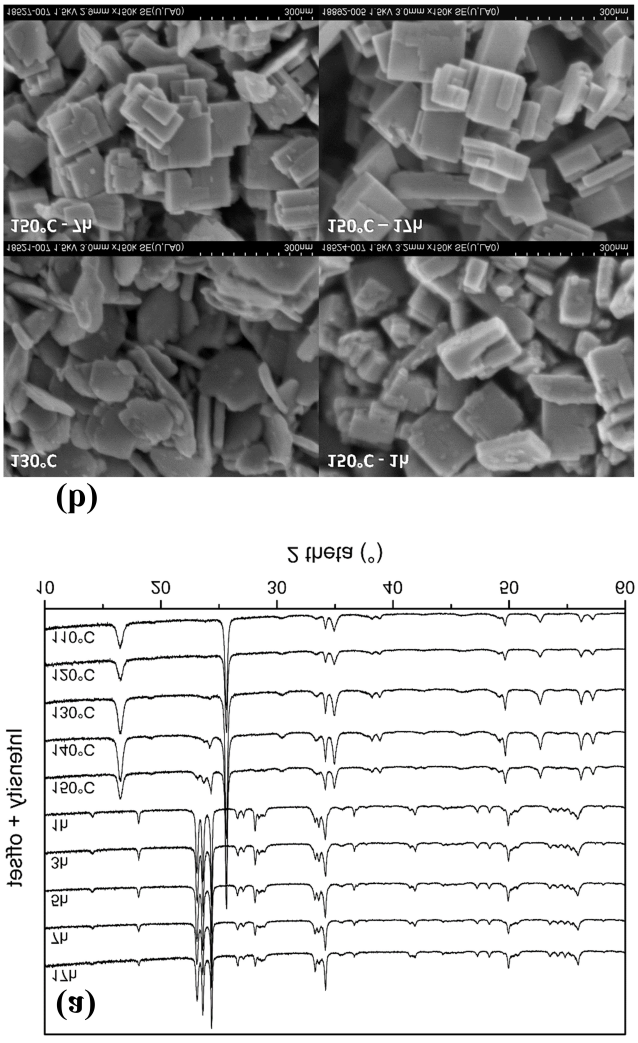

Figure 2. (a) XRD patterns of samples drawn from the reactor at different times during the synthesis of WO_3 at 150 °C and a pH of 1.0. Samples were drawn during the heating process and after reaching the desired synthesis temperature of 150 °C (defined as t = 0 h). (b) SEM images of samples (after withdrawal) after reaching 130 °C and hydrothermal reaction at 150 °C for 1, 7 and 17 h.

observed in small quantities at temperatures of 230 °C and above. At a pH of 2, a significant amount of precipitate is only formed at T = 150 °C and T = 170 °C, which contains the hexagonal crystal phase. Above these temperatures, insufficient precipitate is formed to analyze. XRD patterns of samples synthesized at a pH of 1.5 and 2.0 at 170 °C are depicted in Figure S5. At a pH of 1, pure monoclinic WO_3 is formed at T ≥ 200 °C. When T = 150 °C, a significant amount of $WO_3 \cdot H_2O$ is present, as well as a small amount of $WO_3 \cdot 0.33H_2O$. At T = 170 °C, $WO_3 \cdot H_2O$ is absent, but traces of $WO_3 \cdot 0.33H_2O$ are still left. At a pH of 0.5 formation of $WO_3 \cdot 0.33H_2O$ is not observed anymore, but when the temperature is too low (T = 150 °C), $WO_3 \cdot H_2O$ is still observed. Figure 2a demonstrates that sufficient time at the isothermal stage at 150 °C will result in full transition of $WO_3 \cdot H_2O$ to monoclinic WO_3.

Table 1. Formed crystal phases during microwave-assisted hydrothermal synthesis at different pH and different T, as measured through X-ray diffraction. m-WO_3 is an abbreviation for monoclinic WO_3, h-WO_3 for hexagonal WO_3. N.A. means not available, meaning the amount of formed precipitate was so low that this could not be analyzed.

T / pH	150 °C	170 °C	200 °C	230 °C	250 °C
0.5	60% m-WO_3 40% $WO_3 \cdot H_2O$	m-WO_3	m-WO_3	m-WO_3	m-WO_3
1	62% m-WO_3 32% $WO_3 \cdot H_2O$ 6% $WO_3 \cdot 0.33H_2O$	94% m-WO_3 6% $WO_3 \cdot 0.33H_2O$	m-WO_3	m-WO_3	m-WO_3
1.5	h-WO_3 $WO_3 \cdot 0.33H_2O$	h-WO_3 $WO_3 \cdot 0.33H_2O$	h-WO_3 $WO_3 \cdot 0.33H_2O$	h-WO_3 $WO_3 \cdot 0.33H_2O$ m-WO_3	h-WO_3 $WO_3 \cdot 0.33H_2O$ m-WO_3
2	h-WO_3	h-WO_3	N.A.	N.A.	N.A.

Microwave-assisted hydrothermal synthesis experiments.

The Raman spectroscopy measurements provided *in situ* information on the effect of temperature on crystal phase transitions during hydrothermal synthesis, but required significant analysis time. To reduce the amount of required solution and to enhance the isothermicity of the reactor, reactions were performed in a microwave-assisted hydrothermal reactor, to study the effect of pH at different temperatures on crystal morphology.
As seen from Table 1, the pH value as well as the reaction temperature play a crucial role in determining the final crystal phase of WO_3 that is formed. Generally, a monoclinic WO_3 phase is formed at high temperatures and low pH values during the synthesis. At a pH of 1.5 hexagonal WO_3 and $WO_3 \cdot 0.33H_2O$ are predominantly formed. At this pH, monoclinic WO_3 is only

The structure of the individual phases is also reflected in the overall particle morphology (see Figure S6). In order to compare a set of pure WO_3 samples with similar reaction conditions except for the reaction temperature, the samples synthesized at a pH of 0.5 are further compared. Table 2 shows the BET surface areas in $m^2\ g^{-1}$ as a function of synthesis temperature. An increase in reaction temperature results in a slight decrease in BET surface area of the monoclinic WO_3 samples, which is possibly the result of the nanoplates becoming smoother and larger in size. The sample prepared at 150 °C consists of a mixture with hydrate phase, which causes a slightly higher surface area.

Table 2. BET surface area as a function of temperature of samples synthesized through microwave-assisted hydrothermal synthesis at pH = 0.5.

T (°C)	BET (m^2 g^{-1})	Bandgap (eV)
150	17.61	2.55
170	14.76	2.69
200	13.84	2.69
230	13.44	2.69
250	13.41	2.68

Kubelka-Munk and Tauc plots of the samples obtained by microwave-assisted hydrothermal synthesis at a pH of 0.5 are depicted in Figure 3. The (indirect) bandgaps deducted from the Tauc plots are depicted in Table 2. For each m-WO_3 sample, an identical bandgap of 2.7 eV is calculated, in consistency with literature.[1] For the WO_3 sample synthesized at a pH of 0.5 and T = 150 °C, determining the bandgap is more complicated, as there are two crystal phases present. From the as-obtained Tauc plot, we estimate the bandgap to be at 2.55 eV. The slightly lower bandgap might be the result of H_2O groups in the crystal lattice, inducing defects.

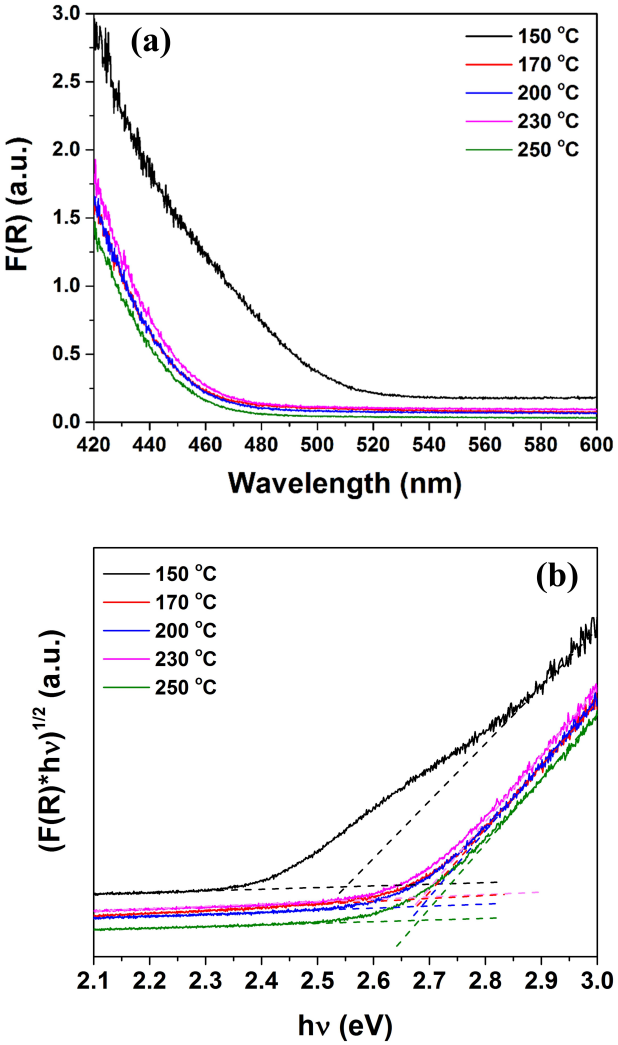

Figure 3. (a) Kubelka-Munk and (b) Tauc plots of WO_3 obtained through microwave-assisted hydrothermal synthesis at pH = 0.5 at variable temperature.

Discussion on crystal phase transformations in (microwave-assisted) hydrothermal synthesis.

As observed in the previous sections, the pH and the synthesis temperature play a crucial role in determining the obtained crystal phase of the WO_3. Here, we discuss the role of these parameters in more detail. At low pH (≤ 1) and temperatures of 170 °C or higher, the final product is phase-pure monoclinic WO_3. This trend is both observed for the 'conventional' hydrothermal synthesis experiments (Figures 1 and S3) and the microwave-assisted hydrothermal synthesis experiments (Table 1). We speculate that the basis for obtaining this phase-pure monoclinic WO_3 lies in the formation of tungstic acid seeds (tungsten oxide hydrates in the form of $WO_3 \cdot 2H_2O$ or $WO_3 \cdot H_2O$) at these low pH values at room temperature, which also involves coordination of citric acid molecules. This is evidenced by the visible formation of a yellow precipitate during the preparation of the solution used in the

hydrothermal synthesis procedure. The formation of such a yellow precipitate is not observed at a pH of 1.5 and 2, nor in the absence of citric acid at any pH. At these conditions, tungsten will be present in the form of a dissolved tungstate rather than a tungsten oxide hydrate. Considering the Pourbaix diagram of tungsten, deprotonation of H_2WO_4 occurs at a pH higher than 2.[20] We speculate that similar effects occur in our experiments at a pH of 1.5 and 2. Tungsten will be present in an anionic form, preventing citric acid to interact properly with these tungsten seeds. This prevents formation of a tungsten precipitate. Unfortunately we were not able to resolve the chemical nature of the interaction of citric acid with the tungstic acid seeds experimentally. Although we can detect citric acid in aqueous solution using Raman spectroscopy (Figure S7), citric acid could unfortunately not be detected in solution during the *in situ* hydrothermal treatment (Figures 1 and S3). Likely, the intensity of the peaks corresponding to tungsten species is much stronger than the intensity of the peaks corresponding with the citric acid in solution. During the hydrothermal synthesis at elevated temperatures, crystal phase transitions $WO_3 \cdot 2H_2O$ à $WO_3 \cdot H_2O$ à m-WO_3 take place due to decomposition of the hydrate phases. A possible explanation for the role of the citric acid in the crystallization of *m*-WO_3 has been provided by Biswas *et al.*[21] Prior to hydrothermal treatment, acidification could result in polycondensation of WO_4^{2-}. However, this can be prevented by the introduction of citric acid. This allows the formation of seeds of WO_3 hydrates. When these are formed, citric acid will adsorb on specific facets of the seeds, changing the order of free energies of the facets. In such a way, the growth rates of the different facets are affected, ultimately resulting in the formation of WO_3 nanoplates.

It is reasonable to assume that the citric acid is decomposed during the hydrothermal synthesis process. This is amongst others evidenced by a slight increase in pressure (Figure S1), which is likely the result of CO_2 formation due to citric acid decomposition. Furthermore, we observe in Figure S3 after 10 hours in the hydrothermal synthesis procedure the formation of broad peaks at 939 and 969 cm^{-1}. Formation of such peaks could be the result of citric acid decomposition in other species, such as acetonedicarboxylic acid and acetoacetic acid.[22]

Photocatalytic activity measurements.

To demonstrate the relevance of this work for photocatalysis, the samples synthesized by the microwave hydrothermal method at a pH of 0.5 were analyzed for photocatalytic activity in the oxidation of propane. As CO_2 was very dominantly formed, the production of CO_2 was taken as a basis for photocatalytic activity. A typical measurement is included in Figure 4. Figure 4a demonstrates the rate of CO_2 formation based on analysis of CO_2 quantity obtained after 10 minutes of illumination, whereas Figure 4b demonstrates the yield of CO_2 as a function of increasing reaction time. In the dark-measurements hardly any CO_2 is formed, whereas considerably large amounts of CO_2 are formed upon illumination at 420 nm. Figure 4a demonstrates that the CO_2 formation rate slightly decreases as a function of increasing light exposure time (runs 3 to 8). The decrease in rate might be explained by poisoning of the catalyst surface by adsorption of oxidation products. A repetition of this particular experiment (runs 13 to 18 in Figure 4a), after the coating was used to construct the curve of Figure 4b, shows stabilization in the CO_2 formation rate takes place to approximately the same value as in runs 3 to 8. Figure 4b shows that initially the relationship between the amount of CO_2 formed and the reaction time is linear. When the same coating was exposed to the same set of experiments (cycle 2 in Figure 4), comparable behavior was observed.

Figure 5 depicts the average rate of CO_2 formation over WO_3 photocatalyst synthesized at variable conditions, corrected for their BET surface area. When the synthesis temperature was 170, 200, 230 or 250 ^oC, the rate is approximately similar (around 6.3 to 7 µmol CO_2 m^{-2} h^{-1}). The sample synthesized at 150 ^oC is considerably less active than the others (around 2.9 µmol CO_2 m^{-2} h^{-1}). Obviously, the main difference between this sample and the others is the presence of both monoclinic WO_3 and $WO_3 \cdot H_2O$, whereas in the other samples only monoclinic WO_3 is present. This underlines that the presence of the $WO_3 \cdot H_2O$ seems detrimental for the photocatalytic activity. A likely explanation for this behavior would be that the hydrate in $WO_3 \cdot H_2O$ acts as a charge carrier recombination trap site, *i.e.* the lifetime of the excited electrons and holes is dramatically reduced.

The hexagonal WO_3 sample synthesized at 170 ^oC and a pH of 2 has been tested on its photocatalytic activity as well. However, the activity under visible light is inferior to its monoclinic counterpart (Figure S8). In previous studies, Nagy *et al.* and Adhikari *et al.* demonstrate that the bandgap of hexagonal WO_3 is larger than the bandgap of monoclinic WO_3.[23] Here, it is very likely that the hexagonal WO_3 also has a larger bandgap than the monoclinic WO_3. Illumination took place at 420 nm, which corresponds to a photon energy of 2.95 eV. It is plausible that the bandgap of the hexagonal WO_3 exceeds 2.95 eV, hence explaining the negligible activity in photocatalytic propane oxidation.

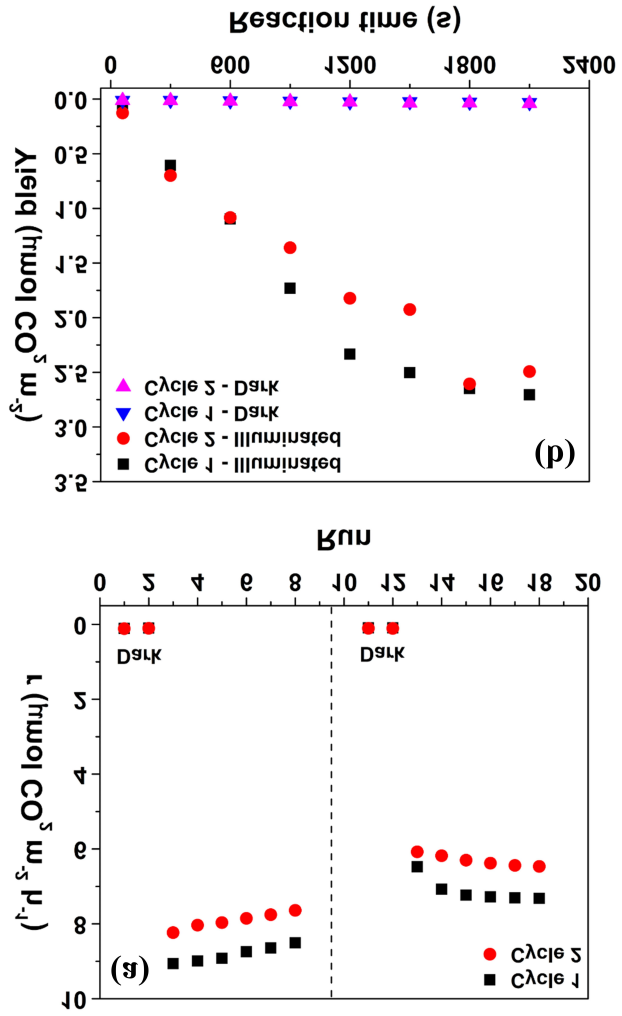

Figure 4. CO_2 formation rates (a) and yield (b) in photocatalytic oxidation of propane in visible light (420 nm) over a coating of WO_3 nanoplates, synthesized at pH = 0.5 and T = 200 °C in a microwave. The same set of experiments was repeated (cycles 1 & 2). The dashed line in (a) represents the moment that the measurements of (b) took place.

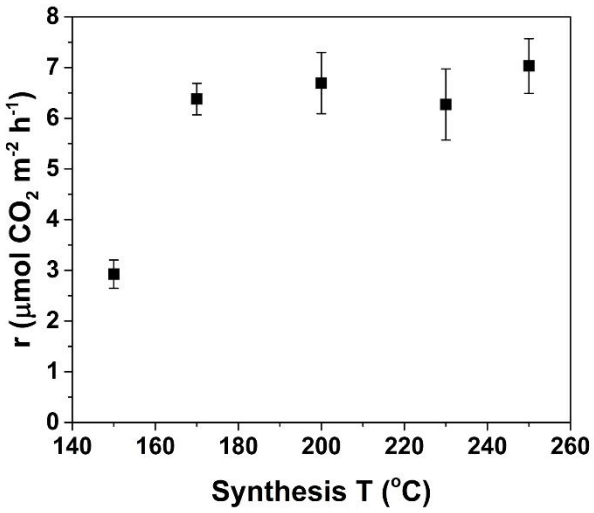

Figure 5. Average CO_2 production rates during photocatalytic oxidation of propane using coatings of WO_3 nanoplates obtained through microwave-assisted hydrothermal synthesis at a pH of 0.5, corrected for BET surface area.

Conclusions

In this manuscript, insight is provided in the phase transformations occurring upon hydrothermal synthesis of WO_3 aqueous sodium tungstate solution containing citric acid as a function of temperature and pH. If the pH is 1 or lower, mainly tungsten oxide dihydrate ($WO_3 \cdot 2H_2O$) is formed. During heating, starting from 70 °C, the tungsten oxide dihydrate is first transformed to tungsten oxide monohydrate ($WO_3 \cdot H_2O$). At temperatures above 150 °C, $WO_3 \cdot H_2O$ is transformed mainly into monoclinic WO_3. To a minor extent, $WO_3 \cdot 0.33H_2O$ is also formed, but this crystal phase is slowly decomposed into monoclinic WO_3 in the isothermal stage. Microwave-assisted hydrothermal synthesis experiments indicate that there is a tipping point in pH in the synthesis: underneath this pH, the dominant crystal phase is monoclinic WO_3, provided the temperature is high enough to prevent formation of hydrated WO_3. Furthermore, BET measurements have demonstrated that an increase in reaction temperature results in more uniform samples, while Kubelka-Munk and Tauc plots indicate that the bandgap remains constant for phase-pure monoclinic WO_3.

The photocatalytic activity of the samples synthesized through microwave hydrothermal synthesis at a pH of 0.5 has been tested in the photo-oxidation of propane under visible light (420 nm). We observe that the synthesis temperature affects the amounts of CO_2 formed: when the synthesis temperature is too low, photocatalytically inactive hydrates ($WO_3 \cdot H_2O$) will be present, resulting in a decrease of photocatalytic activity. When the temperature is sufficiently high, only monoclinic WO_3 is formed and the photocatalytic activity is considerably higher. The monoclinic WO_3 samples did not show a significant difference in photocatalytic activity.

The studies as performed in this paper can contribute greatly to understanding crystal growth of WO_3 using citric acid and to use this in optimizing crystal facet engineering of WO_3. For example,

we have recently published studies on structure-directed deposition of Pt on WO_3 particles synthesized in a Teflon-lined 4748 acid digestion vessel.[24]

Experimental Section

***In situ* Raman spectroscopy of crystal phases during hydrothermal synthesis of WO_3:** All chemicals of analytical grades were purchased from Sigma-Aldrich, Merck and Alfa Aesar. In a typical hydrothermal experiment, 4.33g of sodium tungstate dihydrate ($Na_2WO_4 \cdot 2H_2O$) and 2.60g of citric acid (CA) were dissolved, each in 30 g of Millipore water. The solutions were further diluted in an additional 200 mL of Millipore water and filled into an MED1075 autoclave giving a total W-concentration of 0.05 M and a molar ratio of approximately W/CA = 1:1. The pH was adjusted to 0.5 or 1.0 using concentrated HCl (32%). The solution was heated to the reaction temperature of 150-170 °C with a rate of 1.5 K min^{-1} and kept isothermal at this reaction temperature for 17 hours. During the entire experiment, the solution was stirred at 300 rpm. *In situ* Raman measurements were performed using a Kaiser Optics Raman Spectrometer RXN1 equipped with a fiber-optic probe-head (laser wavelength at 785 nm, 125 mW). Samples were withdrawn from the vessel at different temperatures and reaction times for X-ray diffraction (XRD) and scanning electron microscopy (SEM) investigations of the precipitates, after washing with water and drying. Temperature/pressure profiles of the experiments can be found in the supplementary information (Figure S1). To monitor the pH, an InLab Routine Pro model from Mettler Toledo was used for temperatures up to 80-90 °C. During the hydrothermal synthesis, for temperatures above 120 °C, the pH could also be measured using a ZrO_2 electrode together with a Ag/AgCl reference electrode (both from Corr instruments). The as-prepared products were washed with water, then either with ethanol or a 1:2 water/ethanol mixture and were dried overnight at a maximum temperature of 100 °C.

Microwave-assisted hydrothermal synthesis experiments: Microwave-assisted hydrothermal synthesis studies have been performed with a Multiwave PRO from Anton Paar using 80 ml quartz vessels. In a typical synthesis, 2.64 g of $Na_2WO_4 \cdot 2H_2O$ and 1.68 g of citric acid were each dissolved in 80 mL H_2O. Afterwards, the solutions were mixed together and the pH was adjusted to values in a range of 0.5 to 2 using diluted HCl (the pH was determined using an InLab Routine Pro Model from Mettler Toledo). After dilution with H_2O to a total volume of 160 mL, the solution was equally distributed over four cuvettes, which were placed in the microwave hydrothermal synthesis oven. The reaction was conducted at temperatures in the range of 150 °C to 250 °C for 2 hours using a heating rate of 10 K min^{-1}. It should be noted that the heating rate is different compared to the experiments with the MED1075 autoclave. The phase composition of the products was studied by using powder X-ray diffraction (XRD), using a STOE STADI P transmission diffractometer equipped with a primary focusing germanium monochromator ($CuK_{\alpha 1}$ radiation) and a linear position sensitive detector. Diffraction data were analyzed by whole pattern Rietveld fitting using the program TOPAS (Bruker AXS). With this software, not only can we carefully monitor which crystal phases are formed, but also in which ratio they are present. The morphology was studied by scanning electron microscopy (SEM) using a Hitachi S-4800 electron microscope operating at 1.5 kV in secondary electron (SE) mode. Nitrogen physisorption measurements were performed at liquid N_2 temperature on a Quantachrome Autosorb-6B analyzer. Prior to measurement, the samples were outgassed in vacuum at 150 °C for 3 h. The specific surface area was calculated according to the multipoint Brunauer–Emmett–Teller method (BET). For the WO_3 samples synthesized at a pH of 0.5, the bandgap was determined by employing diffuse reflectance spectroscopy. To this end, a DRS-cell (Harrick, Praying Mentis) and a UV-Vis spectrophotometer (Thermo Scientific, Evolution 600) were combined. Barium sulfate ($BaSO_4$) was used as a reference. From as-measured diffuse reflectance spectra Kubelka-Munk and Tauc plots were constructed. Using the latter, the indirect bandgap was determined by deriving the intersection of the slope and the baseline, as described by Montini *et al.*[25]

Photocatalytic activity measurements: Photocatalytic activity measurements were performed with plate-like WO_3 samples synthesized using microwave-assisted hydrothermal synthesis. Photocatalytic oxidation of propane (C_3H_8), of which the products were analyzed by gas chromatography, was used as prove reaction. To this end a 2 mL batch reactor in combination with an Agilent 7820 GC system (containing a Varian CP7584 column and a Methanizer-FID combination) as described by Fraters *et al*. was used.[18a] Before the samples were loaded into the reaction cell, coatings of these samples on glass substrates (25.3 mm x 25.8 mm) were made through dropcasting, using a stock slurry solution of 3 mL Millipore H_2O (pH = 2, pH adjusted with concentrated HCl and measured using a HI 1332 probe in combination with a pH 209 pH meter from Hanna instruments) with 150 mg of as-synthesized WO_3. The glass substrates were cleaned through sonication in acetone first, then in ethanol, followed by treatment for 30 minutes in a mixture of H_2O, H_2O_2 (≥35%) and NH_4OH (28-30% NH_3 content) with a ratio of 5:1:1. After treatment, the substrates were put on a heating plate preheated at 100 °C. 750 µL of the slurry solution was dropcasted on each glass plate. After evaporation of the water a uniform coating was obtained. To ensure tightness of the reactor cell, coating was removed (by scraping with a spatula) so that an inner circle with a diameter of 1.25 cm remained (corresponding with a sample area of 0.61 cm^2). The mass of the sample present on the coating was calculated to be approximately 7.05 mg.

As-made coatings on glass substrates were loaded into the reaction cell for photocatalytic testing. Prior to the measurements, the batch reactor was purged with a gas mixture containing 80 vol% N_2, 19.5 vol% O_2 and 5000 vol ppm propane (C_3H_8) for a minimum of 21 minutes. Afterwards, the valves of the batch reactor were closed, followed by illumination for 10 minutes with a 420 nm LED (intensity 6.2 mW/cm^2 at the coating surface). Afterwards, the reactor was purged with He and the gas mixture was analysed by gas chromatography. For each coating, the following sequence of runs was performed: i) two runs in the dark, followed by six runs under illumination, ii) a sequence of runs under different illumination times, iii) a sequence of runs under different reaction times in the dark and iv) again, two runs in the dark, followed by six runs under illumination. An area of 0.61 cm^2 was illuminated in the experiments.

We will focus on the formation of CO_2, as selectivity towards this compound was by far the highest. The reaction rate *r* of CO_2 formation (mol g^{-1} h^{-1}) was calculated as follows, inspired by Fraters *et al*.:[18a]

$$r = \frac{P \cdot X_{CO_2} \cdot V}{R \cdot T} \cdot \frac{1}{m \cdot S_{BET}} \cdot \frac{3600}{t} \quad (1)$$

In equation 1, *P* is the pressure inside the batch reactor (Pa), *V* the gas volume inside the reactor (m^3), *R* the gas constant (m^3 Pa mol^{-1} K^{-1}), *T* the temperature inside the reactor (K), *m* the mass of the catalyst (g), S_{BET} the BET surface area of the sample (m^2 g^{-1}), *t* the illumination time (s) and X_{CO_2} the gas fraction of CO_2 present inside the reactor. Our experience is that the WO_3 samples need to stabilize over multiple runs to obtain a constant propane oxidation rate. Therefore, we will focus in this manuscript mainly

on the last three runs of the 4th sequence. From these runs we calculated the average reaction rate of CO_2 formation. By repeating this measurement using either additional measurements on the same coating and/or other coatings, a final average reaction rate including error bars was calculated.

Acknowledgements

This project was funded by the Dutch National Research School Combination Catalysis Controlled by Chemical Design (NRSC-Catalysis). From the University of Twente, we would like to thank Vera Smulders for her help in performing Raman measurements concerning citric acid in aqueous solution. Furthermore, from the Fritz Haber Institute, we would like to acknowledge Jasmin Allan for performing XRD measurements and we would like to thank Frank Girgsdies for his help in analyzing the XRD patterns. Also we want to thank Gisela Weinberg for making HR-SEM images and Maike Hashagen for performing BET surface area measurements.

Keywords: Crystal engineering • Tungsten oxide • Hydrothermal synthesis • Raman spectroscopy • Photocatalysis

[1] a) H. Zheng, J. Z. Ou, M. S. Strano, R. B. Kaner, A. Mitchell, K. Kalantar-Zadeh, *Advanced Functional Materials* **2011**, *21*, 2175-2196; b) J. Kim, C. W. Lee, W. Choi, *Environmental Science and Technology* **2010**, *44*, 6849-6854; c) A. Kudo, Y. Miseki, *Chemical Society Reviews* **2009**, *38*, 253-278.

[2] a) S. H. S. Chan, T. Yeong Wu, J. C. Juan, C. Y. Teh, *Journal of Chemical Technology and Biotechnology* **2011**, *86*, 1130-1158; b) R. Abe, M. Higashi, K. Domen, *ChemSusChem* **2011**, *4*, 228-237.

[3] M. Deepa, A. G. Joshi, A. K. Srivastava, S. M. Shivaprasad, S. A. Agnihotry, *Journal of the Electrochemical Society* **2006**, *153*, C365-C376.

[4] a) H. G. Choi, Y. H. Jung, D. K. Kim, *Journal of the American Ceramic Society* **2005**, *88*, 1684-1686; b) Z. G. Zhao, M. Miyauchi, *Journal of Physical Chemistry C* **2009**, *113*, 6539-6546.

[5] G. Gu, B. Zheng, W. Q. Han, S. Roth, J. Liu, *Nano Letters* **2002**, *2*, 849-851.

[6] M. Regragui, M. Addou, A. Outzourhit, J. C. Bernéde, E. El Idrissi, E. Benseddik, A. Kachouane, *Thin Solid Films* **2000**, *358*, 40-45.

[7] N. Shankar, M. F. Yu, S. P. Vanka, N. G. Glumac, *Materials Letters* **2006**, *60*, 771-774.

[8] B. C. Satishkumar, A. Govindaraj, M. Nath, C. N. R. Rao, *Journal of Materials Chemistry* **2000**, *10*, 2115-2119.

[9] a) J. Zhu, S. Wang, S. Xie, H. Li, *Chemical Communications* **2011**, *47*, 4403-4405; b) J. Wang, E. Khoo, P. S. Lee, J. Ma, *Journal of Physical Chemistry C* **2008**, *112*, 14306-14312; c) R. F. Mo, G. Q. Jin, X. Y. Guo, *Materials Letters* **2007**, *61*, 3787-3790.

[10] a) Z. Gu, H. Li, T. Zhai, W. Yang, Y. Xia, Y. Ma, J. Yao, *Journal of Solid State Chemistry* **2007**, *180*, 98-105; b) Z. Gu, T. Zhai, B. Gao, X. Sheng, Y. Wang, H. Fu, Y. Ma, J. Yao, *Journal of Physical Chemistry B* **2006**, *110*, 23829-23836.

[11] a) X. Su, F. Xiao, Y. Li, J. Jian, Q. Sun, J. Wang, *Materials Letters* **2010**, *64*, 1232-1234; b) J. Wang, P. S. Lee, J. Ma, *Journal of Crystal Growth* **2009**, *311*, 316-319; c) Y. P. Xie, G. Liu, L. Yin, H. M. Cheng, *Journal of Materials Chemistry* **2012**, *22*, 6746-6751.

[12] Z. G. Zhao, Z. F. Liu, M. Miyauchi, *Chemical Communications* **2010**, *46*, 3321-3323.

[13] S. Jeon, K. Yong, *Journal of Materials Chemistry* **2010**, *20*, 10146-10151.

[14] a) Y. Zhao, H. Chen, X. Wang, J. He, Y. Yu, H. He, *Analytica Chimica Acta* **2010**, *675*, 36-41; b) J. Yu, L. Qi, *Journal of Hazardous Materials* **2009**, *169*, 221-227; c) S. K. Biswas, J. O. Baeg, *International Journal of Hydrogen Energy* **2013**, *38*, 3177-3188.

[15] G. Liu, J. C. Yu, G. Q. Lu, H. M. Cheng, *Chemical Communications* **2011**, *47*, 6763-6783.

[16] J. Sungpanich, T. Thongtem, S. Thongtem, *Ceramics International* **2012**, *38*, 1051-1055.

[17] J. Noack, F. Rosowski, R. Schlögl, A. Trunschke, *Zeitschrift fur Anorganische und Allgemeine Chemie* **2014**, *640*, 2730-2736.

[18] a) B. D. Fraters, R. Amrollahi, G. Mul, *Journal of Catalysis* **2015**, *324*, 119-126; b) M. Khajeh Aminian, M. Hakimi, *Catalysis Science and Technology* **2014**, *4*, 657-664.

[19] a) A. G. Souza-Filho, V. N. Freire, J. M. Sasaki, J. Mendes Filho, J. F. Julião, U. U. Gomes, *Journal of Raman Spectroscopy* **2000**, *31*, 451-454; b) A. Baserga, V. Russo, F. Di Fonzo, A. Bailini, D. Cattaneo, C. S. Casari, A. Li Bassi, C. E. Bottani, *Thin Solid Films* **2007**, *515*, 6465-6469; c) M. Gotić, M. Ivanda, S. Popović, S. Musić, *Materials Science and Engineering B: Solid-State Materials for Advanced Technology* **2000**, *77*, 193-201; d) M. F. Daniel, B. Desbat, J. C. Lassegues, B. Gerand, M. Figlarz, *Journal of Solid State Chemistry* **1987**, *67*, 235-247.

[20] E. Patrick, M. E. Orazem, J. C. Sanchez, T. Nishida, *Journal of Neuroscience Methods* **2011**, *198*, 158-171.

[21] S. K. Biswas, J. O. Baeg, S. J. Moon, K. J. Kong, W. W. So, *Journal of Nanoparticle Research* **2012**, *14*.

[22] C. H. Munro, W. E. Smith, M. Garner, J. Clarkson, P. C. White, *Langmuir* **1995**, *11*, 3712-3720.

[23] a) D. Nagy, D. Nagy, I. M. Szilagyi, X. Fan, *RSC Advances* **2016**, *6*, 33743-33754; b) S. Adhikari, D. Sarkar, *RSC Advances* **2014**, *4*, 20145-20153.

[24] K. Wenderich, A. Klaassen, I. Siretanu, F. Mugele, G. Mul, *Angewandte Chemie International Edition* **2014**, *53*, 12476-12479.

[25] T. Montini, V. Gombac, A. Hameed, L. Felisari, G. Adami, P. Fornasiero, *Chemical Physics Letters* **2010**, *498*, 113-119.

Entry for the Table of Contents

FULL PAPER

***In situ* Raman** spectroscopy and microwave-assisted hydrothermal synthesis experiments show a pH of 0.5 and a temperature above 170 ºC are required to obtain plate-like, phase-pure monoclinic WO_3 nanoplates from a solution containing sodium tungstate and citric acid. These phase-pure samples show better photocatalytic performance in the oxidation of gaseous propane than samples containing hydrated WO_3 phases.

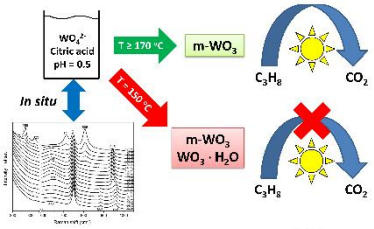

Crystal engineering

Kasper Wenderich, Johannes Noack, Anne Kärgel, Annette Trunschke, Guido Mul*

Page No. – Page No.

Effect of temperature and pH on phase transformations in citric acid-mediated hydrothermal growth of tungsten oxide